Applied Catalysis B: Environmental 184 (2016) 182–190

Contents lists available at ScienceDirect

Applied Catalysis B: Environmental

journal homepage: www.elsevier.com/locate/apcatb

Synergistic promotion of solar-driven H_2 generation by three-dimensionally ordered macroporous structured TiO_2-Au-CdS ternary photocatalyst

Heng Zhao [a], Min Wu [a,**], Jing Liu [a], Zhao Deng [a], Yu Li [a], Bao-Lian Su [a,b,c,*]

[a] Laboratory of Living Materials at the State Key Laboratory of Advanced Technology for Materials Synthesis and Processing, Wuhan University of Technology, 122 Luoshi Road, 430070 Wuhan, Hubei, China
[b] Laboratory of Inorganic Materials Chemistry (CMI), University of Namur, 61 rue de Bruxelles, B-5000 Namur, Belgium
[c] Clare Hall College, University of Cambridge, Cambridge, UK

ARTICLE INFO

Article history:
Received 10 July 2015
Received in revised form
10 November 2015
Accepted 16 November 2015
Available online 30 November 2015

Keywords:
3DOM
TiO_2
Au nanoparticles
CdS
H_2 evolution
Efficient electron transfer

ABSTRACT

A ternary photocatalyst TiO_2-Au-CdS based on three-dimensionally ordered macroporous TiO_2 (3DOM TiO_2) was successfully prepared to enhance the light absorption, extend the light responsive region, reduce the recombination rate of charge carriers and promote the efficiency of water splitting H_2 evolution ultimately. The obtained 3DOM TiO_2-Au-CdS powder has a pure anatase phase of TiO_2 and greenockite structured CdS according to the XRD results and TEM analysis. Au nanoparticles (AuNPs) and CdS were evenly distributed in the 3DOM structure which enhances H_2-generation rate under visible light by improving light harvesting and utilizing its mass transfer facilitation. As a result, the hydrogen generation rate (1.81 mmol h^{-1} g^{-1}) using 3DOM TiO_2-Au-CdS photocatalyst under visible light irradiation was 13-fold higher than the binary 3DOM TiO_2-CdS reference photocatalyst. Under ultraviolet-visible light, the photogenerated electrons in TiO_2 would be transferred to recombine with the holes of CdS and under visible light, electrons would move to the conduction band (CB) of TiO_2 from CdS via AuNPs. The two different types of internal electron-transfer process in the ternary photocatalyst under ultraviolet and visible light were proposed respectively and both would efficiently reduce the recombination rate of photogenerated electrons and holes thus stimulate H_2 evolution rate. The present work demonstrated an excellent example of the synergistic effect of the light absorption enhancement by 3DOM structure, the photosensitizing and electron reservoir effect of AuNPs and the reduction of recombination rate of charge carriers by CdS to highly promote the photocatalytic activity in water splitting reaction.

1. Introduction

The global energy crisis and environment problems have become increasingly prominent as the fossil fuel is continuously consumed and hydrogen as a clean, storable and environmentally friendly fuel is recognized as the most promising substitute for fossil fuel. Since Fujishima and Honda firstly reported the photoelectrolysis of water over TiO_2, solar driven photocatalytic water splitting over semiconductors to produce hydrogen has been attracting extensively research attention [1–4]. Four facets have been considered to affect the photocatalytic performance of H_2 evolution by water splitting: light absorption, photogenerated charge separation and migration, and redox reactions on the surface of semiconductor. For semiconductor photocatalysts, TiO_2 is recognized as one of the most popular candidates due to its high chemical stability, nontoxicity and low cost [5,6]. However, two major limitations hamper the application of TiO_2: (1) its large bandgap (3.2 eV for anatase phase) restricting its utilization in the visible light zone of the solar spectrum [7] and (2) the high recombination rate of photogenerated electrons and holes leading to a low quantum yield and poor photocatalytic activity [8]. Considerable researches have been conducted to find the solutions to the two problems cited above. Combining TiO_2 with narrow band-gap semiconductors such as CdS [9] and MoS_2 [10] to form a heterostructure would be an effective method to extend the light absorption of TiO_2 to the visible portion

* Corresponding author at: Laboratory of Living Materials at the State Key Laboratory of Advanced Technology for Materials Synthesis and Processing, Wuhan University of Technology, 122 Luoshi Road, Hubei, Wuhan, 430070, China and Laboratory of Inorganic Materials Chemistry, University of Namur, 61 rue de Brussels, B-5000, Namur, Belgium.
** Corresponding author.
E-mail addresses: minwu@whut.edu.cn (M. Wu), baoliansu@whut.edu.cn, bao-lian.su@unamur.be (B.-L. Su).

http://dx.doi.org/10.1016/j.apcatb.2015.11.018
0926-3373/

of the solar spectrum [11]. To improve the life of photogenerated electron-hole pairs, some precise metals as electron reservoirs could be introduced to the surface of TiO_2 to gather the photogenerated electrons, thus efficiently reduce the recombination of charge carriers. Serrano et al. deposited Pt on the surface of ordered mesoporous TiO_2 and the as-fabricated photocatalyst showed higher H_2 evolution under ultraviolet light irradiation [12]. Meanwhile, the surface plasmon resonance (SPR) of noble metal nanoparticles can also improve the photoactivity of TiO_2 [13]. Butburee et al. prepared a new type of plasmonic metal@TiO_2 (metal = Pd and Au) core–shell structure to utilize the SPR effect to enhance the photocatalytic degradation of phenol. In addition to these compositional modifications, using the slow photon effect, a structure effect in three dimensionally ordered macroporous (3DOM, also called photonic crystals) structure to enhance the light harvesting could also promote the photoreactivity [14–20]. Zhang et al. coupled SPR effect of AuNPs with slow photon effect of TiO_2 photonic crystals and proved the synergistic enhancement for photoelectrochemical water splitting activity [21]. The design of ternary photocatalyst TiO_2-Au-CdS has been successfully adopted and fabricated by several groups to promote the photocatalytic hydrogen evolution [22–26], in which the structures of TiO_2 substrate were designed to be nanorod and nanoparticle. Compared with 3DOM structure, the above nanostructures play a relatively weak role in the light harvesting during the photocatalytic reactions. However, it is almost rare using 3DOM structured ternary photocatalyst for hydrogen evolution. Most recently, Wei et al. fabricated the ternary photocatalyst TiO_2-Au-CdS based on 3DOM structure, whereas, the application of the prepared samples was to reduce CO_2 to obtain methane [27]. To the best of our knowledge, this ternary photocatalyst is in favor of reducing water for hydrogen compared with CO_2 as the hydrogen generation is the dynamically favoured reaction and the hydrogen can't be avoided in the process of reducing CO_2 with H_2O under ultraviolet light irradiation.

Hence, it is novel to study a ternary composite photocatalyst TiO_2-Au-CdS based on 3DOM TiO_2 which could be advantageous to the light absorption enhancement, the light responsive region extension and the recombination rate of charge carrier reduction simultaneously. CdS can be adopted to combine with TiO_2 due to its narrow band-gap (2.4 eV), which could extend the light response range to visible region. Meanwhile, the conduction band and valence band (VB) of CdS are capable of completing both the reduction and oxidation of water under visible-light irradiation [28]. To efficiently promote photogenerated electron-hole pairs separation, AuNPs serving as electron reservoirs and photosensitizers as a crucial component can be introduced to this ternary photocatalyst. At the same time, AuNPs could be photosensitized to improve light harvesting due to the presence of surface plasmon resonance (SPR) [13]. 3DOM structure as the skeleton of the ternary photocatalyst could provide the multi-advantages by the periodic structure with large and continuously adjustable pore sizes [29–34]. The slow photon effect, the favorable electron migration to the surface of TiO_2 and excellent accessibility of reactants and light to 3DOM structure are expected to enhance the performance of visible light-driven water splitting of some effects.

In this work, the three-component 3DOM TiO_2-Au-CdS photocatalyst was successfully fabricated and did exhibit highly improved activity for photocatalytic hydrogen generation rate ($1.81\ mmol\ h^{-1}\ g^{-1}$) under visible light irradiation, 13-fold higher than the binary structure 3DOM TiO_2-CdS as reference sample and as compared to the CdS/TiO_2 composite ($0.11\ mmol\ h^{-1}\ g^{-1}$) fabricated by Jang [35]. This as-fabricated ternary photocatalyst provides a transfer path of the internal electrons from CdS to TiO_2 via Au nanoparticles, which significantly enhances the photocatalytic activity for water splitting. In addition, the role of 3DOM structure enhancing H_2-genenration rate is also confirmed. The present work tries to shed light on the development of solar-driven photocatalyst by the combination of narrow band-gap semiconductor and metallic nanoparticles with 3DOM TiO_2 structure, utilizing the features of enhanced visible light sensitivity and absorption, efficient electron-hole separation and excellent reactant and light accessibility.

2. Experimental materials and methods

2.1. Materials

Styrene, ethanol, tetraisopropyl titanate (TIPT), sodium sulfide nonahydrate, sodium citrate dihydrate, sodium sulfite, cadmium nitrate tetrahydrate,were purchased from Aldrich. Gold chloride solution was purchased from Alfa Aesar.

2.2. Colloidal sphere preparation

Surfactant-free emulsion polymerization method was applied to prepared polystyrene (PS) spheres. Styrene was washed three times by using 2 M NaOH to remove the inhibitors. Prewashed styrene (15 mL) and water (200 mL) were heated to 85 °C in an oil bath under a N_2 atmosphere, stirring at a certain speed for 0.5 h. The initiator $K_2S_2O_8$ (0.25 g) was added to activate the polymerization. The reaction was stopped after 3 h by cooling the container and making the air through the system. PS template was obtained directly by using low speed centrifugation of PS spheres.

2.3. Preparation of 3DOM TiO_2

The method of preparing the 3DOM TiO_2 was according to our previous report [32]. The precursor was composed of ethanol (5 mL), hydrochloric acid (1 mL), titanium (IV) isopropoxide (5 mL), and water (2 mL). The mixture was added to a beaker and stirred at room temperature for 5mins. Dried PS template (5 g) was placed on a filter paper in a Buchner funnel, and the precursor was added to the PS templates during suction applied to the Buchner funnel. After air drying the mixture of precursor and template for 48 h, calcination in air was applied to remove the PS template. The sample was stabilized at 300 °C for 2 h, 400 °C for 2 h and 550 °C for 2 h using a heating rate 2 °C/min.

2.4. Decoration of Au nanoparticles on the 3DOM TiO_2

AuNPs was prepared by using citrate reduction of $HAuCl_4$ in water. (10^{-2} g/L) $HAuCl_4$ aqueous solution was heated to 110 °C and 0.5 g 3DOM TiO_2 was immersed into the $HAuCl_4$ aqueous solution rigorous stirring for 0.5 h. Trisodium citrate aqueous solution (1.5 mL 10 g/L) was added to the flask and another 1.5 mL was added after 15 min. The mixture was stirred for 1 h under 110 °C and cooled down to room temperature. The dark purple 3DOM TiO_2-Au was obtained after filtering the mixture.

2.5. Fabrication of 3DOM TiO_2-Au-CdS

3DOM TiO_2-Au-CdS sample was prepared by chemical bath deposition (CBD) method. 3DOM TiO_2-Au sample was dipped in a 0.05 M $Cd(NO_3)_2$ aqueous solution rigorous stirring for 0.5 h and then 0.05 M Na_2S aqueous solution was added. 3DOM TiO_2-Au-CdS was obtained after filtration and washed with DI water.

2.6. Characterization

The sample morphology and structure of the 3DOM were observed with a field-emission scanning electron microscope (SEM, Hitachi S-4800) with an energy-dispersive X-ray (EDX) analysis

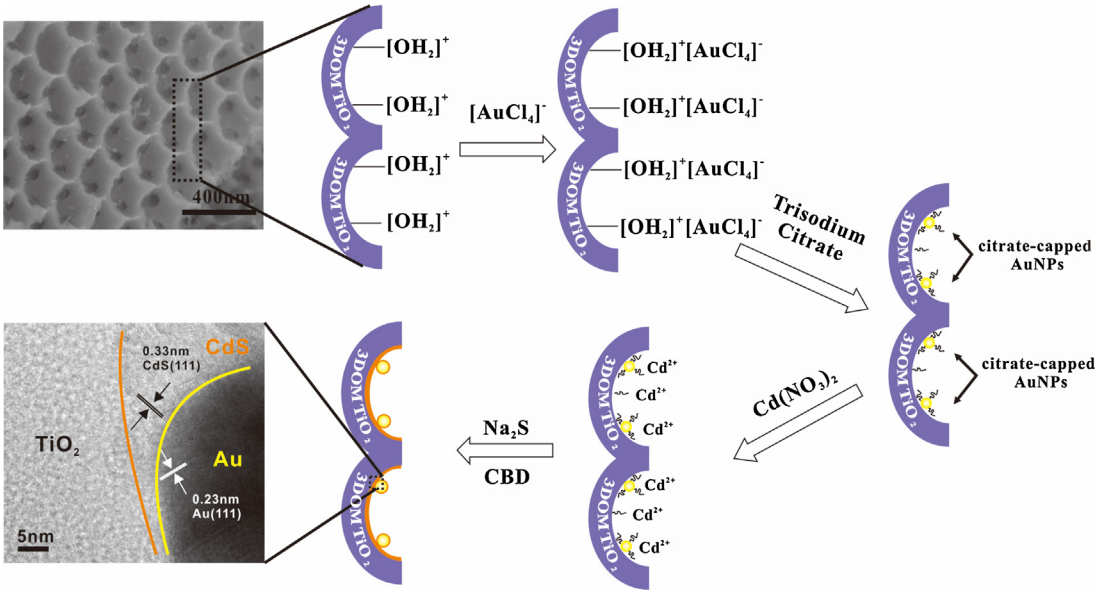

Fig. 1. Schematic illustration of the fabrication processes for 3DOM TiO_2-Au-CdS.

system and a transmission electron microscope (TEM, JEOL JEM 2100F). The high angle annular dark field (HAADF) and energy-dispersive X-ray spectroscopy (EDS) were acquired on a FEI Talos F200X. The crystalline phase of the samples were examined by power X-ray diffraction (XRD, D8 ADVANCE) equipped with a Cu anode X-ray tube (Cu KαX-rays, λ = 1.54056 Å). X-ray photoelectron spectroscopy (XPS) was worked out with a customized X-ray photoelectron spectrometer (VG Multilab 2000-X equipped with a monochromatic Al Kα source). The UV–vis absorption spectra were collected by SHIMADZU UV–vis spectrophotometer in the spectral range 200–800 nm. The Brunauer–Emmett–Teller (BET) specific surface areas of the powders were analyzed in a Micrometrics Tri Star II 3020 nitrogen adsorption-desorption apparatus. Photoluminescence (PL) spectra were recorded using fluorescence spectrophotometer (PerkinElmer LS-55) and the excitation wavelength was set at 400 nm. The actual content of gold was measured by the Inductively Coupled Plasma Emission Spectrometer (ICP-AES, PerkinElmer Optima 4300DV).

2.7. Photocatalytic water splitting for H_2 evolution

The photocatalytic reactions were carried out in a closed circulation system using a PLS-SXE-300C lamp with a UV light intensity of 34 mW/cm^2 and visible light intensity of 158 mW/cm^2. 0.1 g sample was immersed in an aqueous solution containing 0.1 M Na_2S and 0.1 M Na_2SO_3 as the sacrificial agents. The mixture was sealed in a quartz vessel and stirred during photoreaction. After degassing, the vessel was under irradiation of visible light (420–780 nm) and UV–vis light (250–780 nm). The gas products were analyzed periodically by an Agilent 7890A gas chromatograph (GC) with a thermal conductivity detector (TCD).

3. Results and discussion

The ternary photocatalyst 3DOM TiO_2-Au-CdS was prepared by a four steps process (see Fig. 1). First, PS spheres were self-assembled into opals with a face-centered cubic (FCC) structure using low speed centrifugation. The titanium isopropoxide precursor was then added to fill the voids of the PS templates. The penetration and hydrolysis rates of the precursor determine the quality of the final 3DOM structure. The acidity controls the hydrolysis rate of titanium alkoxide. The obtained 3DOM TiO_2 was immersed in the $HAuCl_4$ aqueous solution and citrate reduction was used to decorate AuNPs on the surface of 3DOM TiO_2 evenly. The obtained AuNPs are capped with citrate ions and will catch Cd^{2+} due to the Coulomb force. Finally, S^{2-} substitutes for citrate ions to form CdS on the surface of AuNPs and TiO_2.

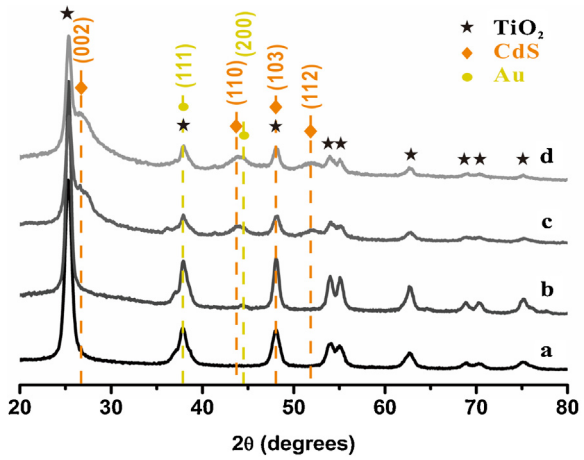

Fig. 2. XRD patterns of (a) 3DOM TiO_2, (b) 3DOM TiO_2-Au, (c) 3DOM TiO_2- CdS, (d) 3DOM TiO_2-Au-CdS.

XRD patterns of 3DOM TiO_2, 3DOM TiO_2-Au, 3DOM TiO_2- CdS and 3DOM TiO_2-Au-CdS are shown in Fig. 2 respectively. For the 3DOM TiO_2 (Fig. 2a), we observed the characteristic diffraction peaks of anatase TiO_2 and good crystallinity. The only crystalline phase observed at a calcination temperature of 550 °C was anatase phase and the average crystallite size of TiO_2 was approximately 10 nm calculated by using Scherrer's equations [36]. The peak at 38.2° and 44.4° (marked by ● in Fig. 2b and d) were corresponding to Au (1 1 1) and (2 0 0) respectively, indicating the successful decoration of AuNPs in the structure of 3DOM TiO_2. Note that the TiO_2 (0 0 4) peak overlaps with Au (1 1 1) peak at 38.2° (2θ). The intensity of Au (2 0 0) peak was very low presumably due to the relatively low incorporation amount of the AuNPs [21]. In addition, a typical XRD pattern for greenockite structured CdS (marked by ♦ in Fig. 2c

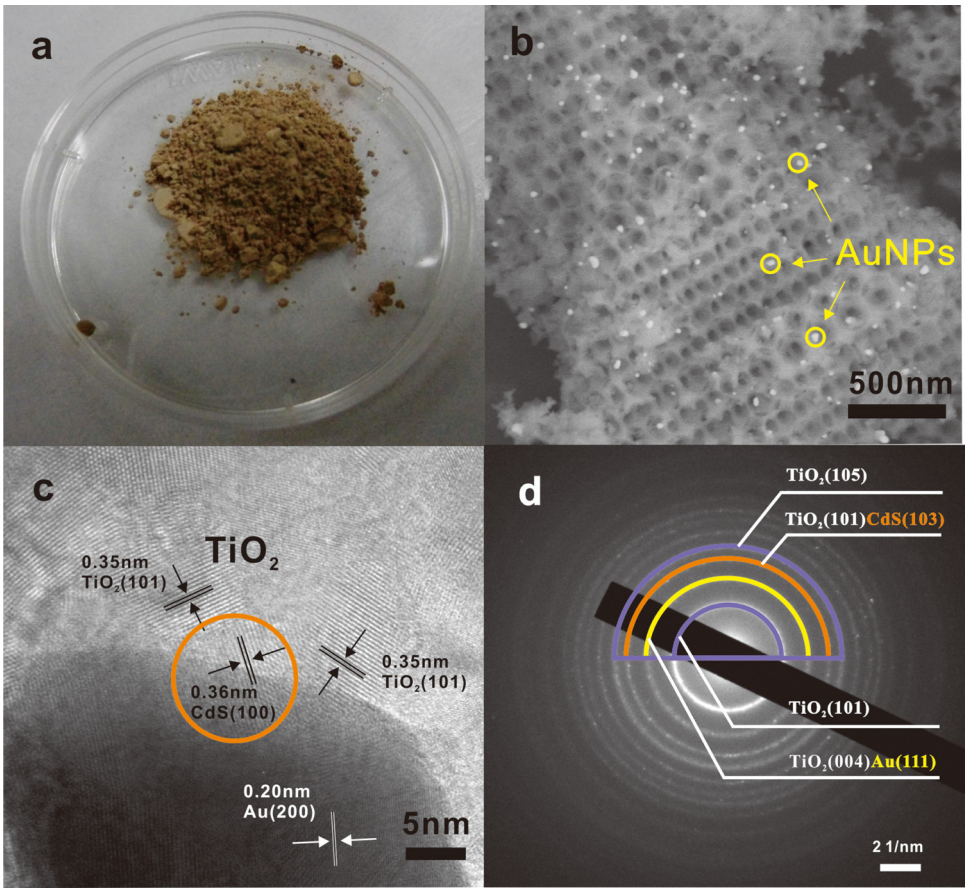

Fig. 3. (a) Photograph, (b) Back Scattered Electron (BSE), (c) High-resolution TEM (HRTEM), (d) Selected Area Electron Diffraction (SAED) images of 3DOM TiO_2-Au-CdS.

and d) was found with crystallographically preferred orientations, indicating the presence of CdS on the prepared photocatalysts.

As shown in Fig. 3a, the obtained 3DOM TiO_2-Au-CdS is yellow in color, suggesting that it can absorb a considerable portion of visible light. The AuNPs and CdS dispersion in the 3DOM TiO_2-Au-CdS was characterized by SEM and TEM. It is clearly seen that the prepared sample is an assembly of highly uniform three dimensionally ordered macroporous structure (Fig. 3b and Fig. S1). The back scattered electron (BSE) image taken by SEM (the bright white spots circled in Fig. 3b represent AuNPs) shows AuNPs are evenly distributed on the surface of 3DOM TiO_2 and the average size of AuNPs is around 30 nm measured from TEM images. Compared with the smaller AuNPs (3–5 nm), the 30 nm AuNPs are not easier to aggregate as the surface energy is relatively lower. Besides, the as-fabricated AuNPs are covered with citrate ions which contribute to restrain the aggregation of AuNPs. The actual content of AuNPs in the ternary photocatalyst is around 0.6% measured by the Inductively Coupled Plasma Emission Spectrometer (ICP-AES). Fig. 3c shows the presence of intimate contacts between Au and CdS nanoparticles, confirming our proposal (Fig. 1) that due to the interaction of Cd^{2+} with the citrate-capped AuNPs, the CdS nanoparticles will be formed around AuNPS. Meanwhile, the relative position of these three components can be also identified. The gold nanoparticles existing between TiO_2 and CdS play a dual-role as electron relay and plasmonic photosensitizer [11]. This close contact between metal and semiconductor can enhance the charge transfer between them, and thus the photocatalytic efficiency [37]. The high-resolution TEM image (Fig. 3c) shows the lattice fringes of each component, thus indicating the highly crystalline nature of CdS, AuNPs and TiO_2. The lattice fringe with a D-spacing of 0.20 nm belongs to the (200) lattice plane of Au. Meanwhile, the lattice fringes with D-spacing of 0.36 nm can be assigned to the (1 0 0) lattice plane of greenockite structured CdS, respectively. The lattice fringe with a D-spacing of 0.35 nm is corresponding to the (1 0 1) lattice plane of anatase TiO_2. The selected area electron diffraction (SAED) pattern is shown in Fig. 3d. The labels from the lower position to the uppers are, respectively, which is in good agreement with the XRD results.

The element distribution maps of 3DOM TiO_2-Au-CdS are shown in Fig. 4. The high angle annular dark field (HAADF) and elemental maps confirm the co-existence of Au, Cd and S and prove that they are homogeneously dispersed on 3DOM TiO_2. The mapping image of S shows AuNPs are capped with CdS, which further confirms that S^{2-} substitutes for citrate ions to form CdS on the surface of AuNPs (shown in Fig. 1). The peak at around 1375 cm^{-1} disappeared in infrared spectra (Fig. S2) for 3DOM TiO_2-Au-CdS also suggests that citrate ions have been substituted by S^{2-}.

Fig. 5 shows the UV–vis absorption spectra of 3DOM TiO_2, 3DOM TiO_2-CdS and 3DOM TiO_2-Au (two components), 3DOM TiO_2-Au-CdS (three components), respectively. All the samples are of the same size and thickness. For pure 3DOM TiO_2 (spectrum a), the strong absorption at wavelength range below 400 nm matches the intrinsic interband transition absorption of pure anatase TiO_2, showing its UV absorption character. 3DOM TiO_2-Au composite (spectrum b) shows a broad peak at 550 nm, corresponding to surface plasmon resonance (SPR) absorption of Au nanoparticles, which could be tuned by varying their size, shape and surrounding environment [38,39]. The shape and position are consistent with 30 nm AuNPs loaded on TiO_2 reported by Kochuveedu [40]. The absorption edge at ~550 nm in spectrum *c* represents the absorption of CdS, which is in agreement with CdS/TiO_2 nano-bulk photocatalyst reported by Jang [41]. After the deposition of CdS on

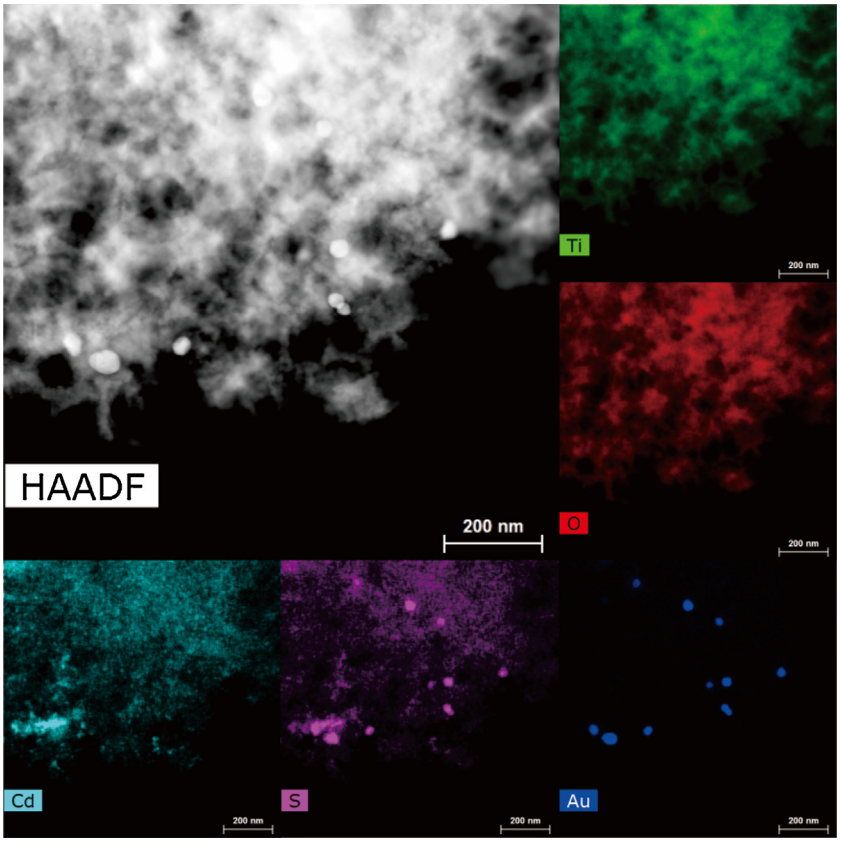

Fig. 4. Energy-dispersive X-ray spectroscopy (EDX) elemental mapping images of 3DOM TiO_2-Au-CdS.

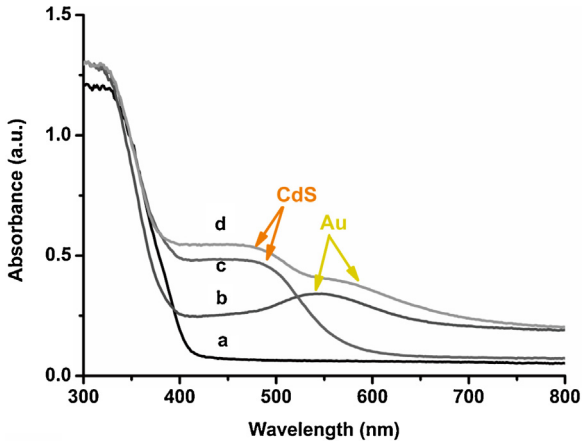

Fig. 5. UV–vis absorption spectra obtained from (a) 3DOM TiO_2, (b) 3DOM TiO_2-Au, (c) 3DOM TiO_2-CdS and (d) 3DOM TiO_2-Au-CdS.

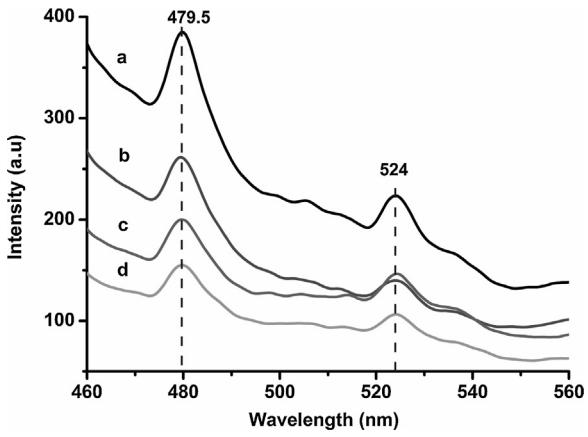

Fig. 6. Photoluminescence (PL) spectra of (a) 3DOM TiO_2, (b) 3DOM TiO_2-Au, (c) 3DOM TiO_2-CdS, (d) 3DOM TiO_2-Au-CdS.

Au nanoparticles (spectrum d), the SPR absorption peak of AuNPs red-shifts to 570 nm because of the strong electromagnetic coupling of Au and CdS [42]. This implies that CdS with higher dielectric constant (vs air) directly contacting with AuNPs would lead to this red shift of the SPR band [22,23].

In the semiconductor materials, electrons would be excited under the irradiation of certain wavelength and induce light emission called fluorescence during the recombination with holes. PL emission spectrum has been widely applied in the study of photocatalysis because it can supply meaningful information about semiconductor materials such as surface oxygen or metal vacancies and the efficiencies of charge carrier migration and transfer [43,44]. Since the 3DOM structure is designed to enhance the light harvesting due to the slow photon effect rather than promote charge carrier separation, the composition of the photocatalyst is the key point affecting the recombination of photogenerated electrons and holes. From the intensity of fluorescence, the enhancement of charge carrier separation could be identified. Fig. 6 shows the PL spectra of as-fabricated 3DOM TiO_2 (spectrum a), 3DOM TiO_2-Au (spectrum b), 3DOM TiO_2-CdS (spectrum c) and 3DOM TiO_2-Au-CdS (spectrum d) under an excitation wavelength of 400 nm. All the spectra have same emission peaks at 479.5 nm and 524 nm, which can be assigned to the radiative recombination of self-trapped exciton luminescence due to the oxygen vacancies of TiO_2 [45–50]. It is observed that the PL intensity of 3DOM TiO_2 (spectrum a) has been largely reduced after the AuNPs decoration. This is mainly attributed to the photogenerated electrons in the conduction band

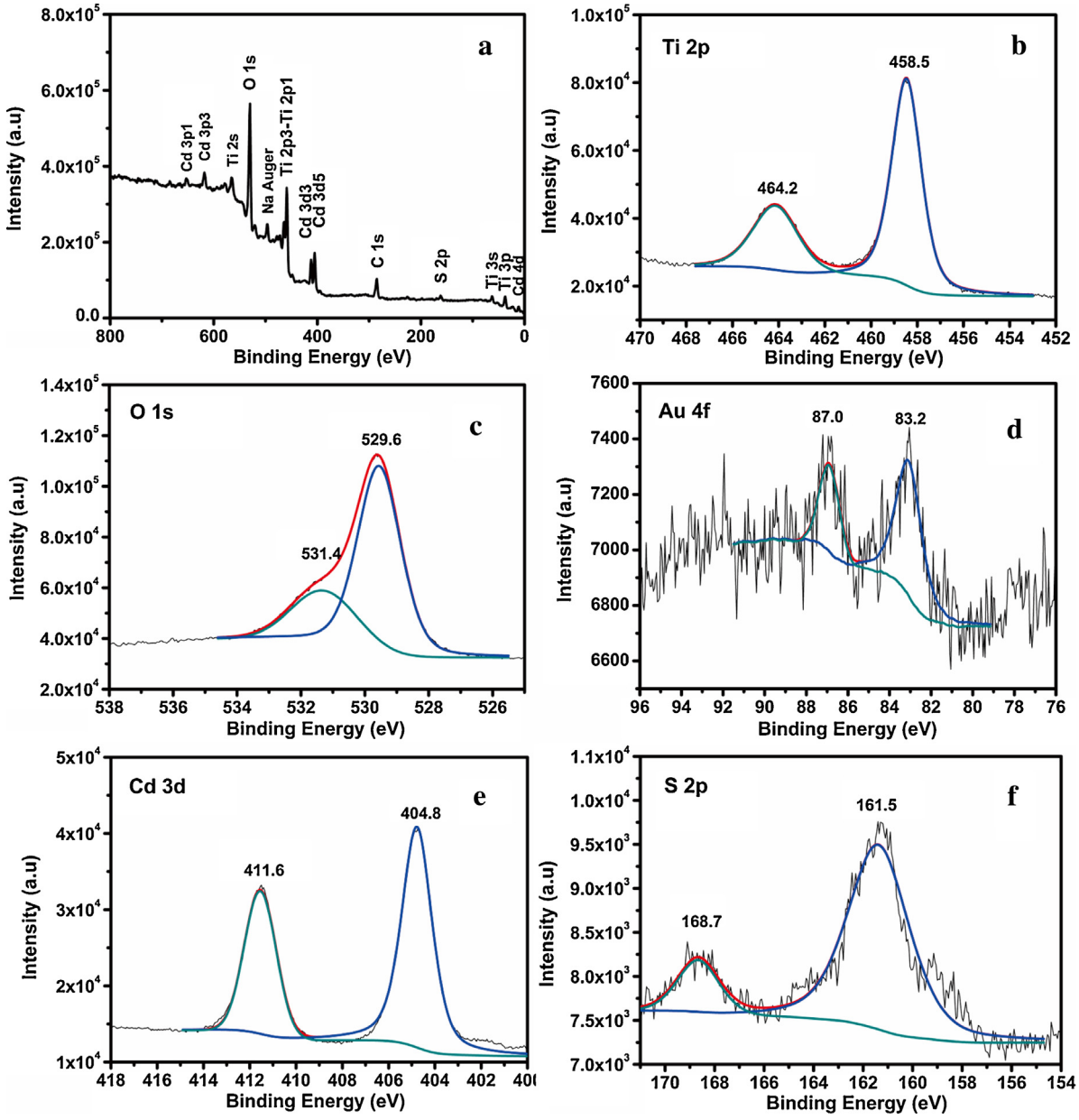

Fig. 7. (a) XPS survey scan for 3DOM TiO_2-Au-CdS over a large energy range at low resolution, High-resolution XPS core level spectra of (b) Ti 2p, (c) O 1s, (d) Au 4f, (e) Cd 3d, (f) S 2p.

of TiO_2 are attracted to AuNPs and hence the charge separation is enhanced compared to pure 3DOM TiO_2 [51]. The 3DOM TiO_2-CdS exhibits similarly lessened intensity, which is possibly ascribed to the suitable band structures between TiO_2 and CdS; the CB of TiO_2 is less negative than the CB of CdS. Therefore, the photogenerated electrons would transfer to the CB of TiO_2 and the separation of electron–hole pairs is improved, indicating the recombination of photoinduced carriers is hampered [52]. The ternary photocatalyst shows a further reduced intensity indicating the heterostructure is formed and the photogenerated electrons in TiO_2 are transferred to CdS through AuNPs and this unique internal electron-transfer of ternary photocatalyst would efficiently reduce the recombination of photogenerated carriers of TiO_2 [22].

The XPS was carried out to further determine the chemical composition and the surface states of the as-fabricated photocatalyst. The general scan spectrum of XPS (Fig. 7a) of 3DOM TiO_2-Au-CdS over large energy range at low resolution shows sharp XPS peaks for Ti, O, Cd, S and C. The XPS peak of Au at low resolution is not obvious as AuNPs are capped with CdS according to EDX result besides of the low content of AuNPs. The detected carbon mainly came from the adventitious hydrocarbon from XPS instrument itself. The high-resolution Ti2p, O1s, Au4f, Cd3d and S2p XPS spectra of 3DOM TiO_2-Au-CdS are shown in Fig. 7. The spin-orbit components (2p3/2 and 2p1/2) of Ti2p peak were well deconvolved by two peaks at 458.5 eV and 464.4 eV respectively with a splitting energy of 5.7 eV, presenting Ti^{4+} species in a tetragonal structure (Fig. 7b). The O1s core level spectrum is asymmetric; besides the main peak of O1s located at about 529.6 eV corresponding to lattice oxygen of TiO_2, a shoulder peak at higher binding energy could be identified. The peak at 531.5 eV should be attributed to the surface species such as Ti—OH and Ti—O—O- (Fig. 7c) [53]. The peaks observed at 83.5 and 87.4 eV were ascribed to metallic gold (Fig. 7d). The Cd3d5/2 and Cd3d3/2 peaks centered at 404.8 and 411.6 eV with a spin-orbit separation of 6.6 eV can be assigned to Cd^{2+} of CdS nanoparticles

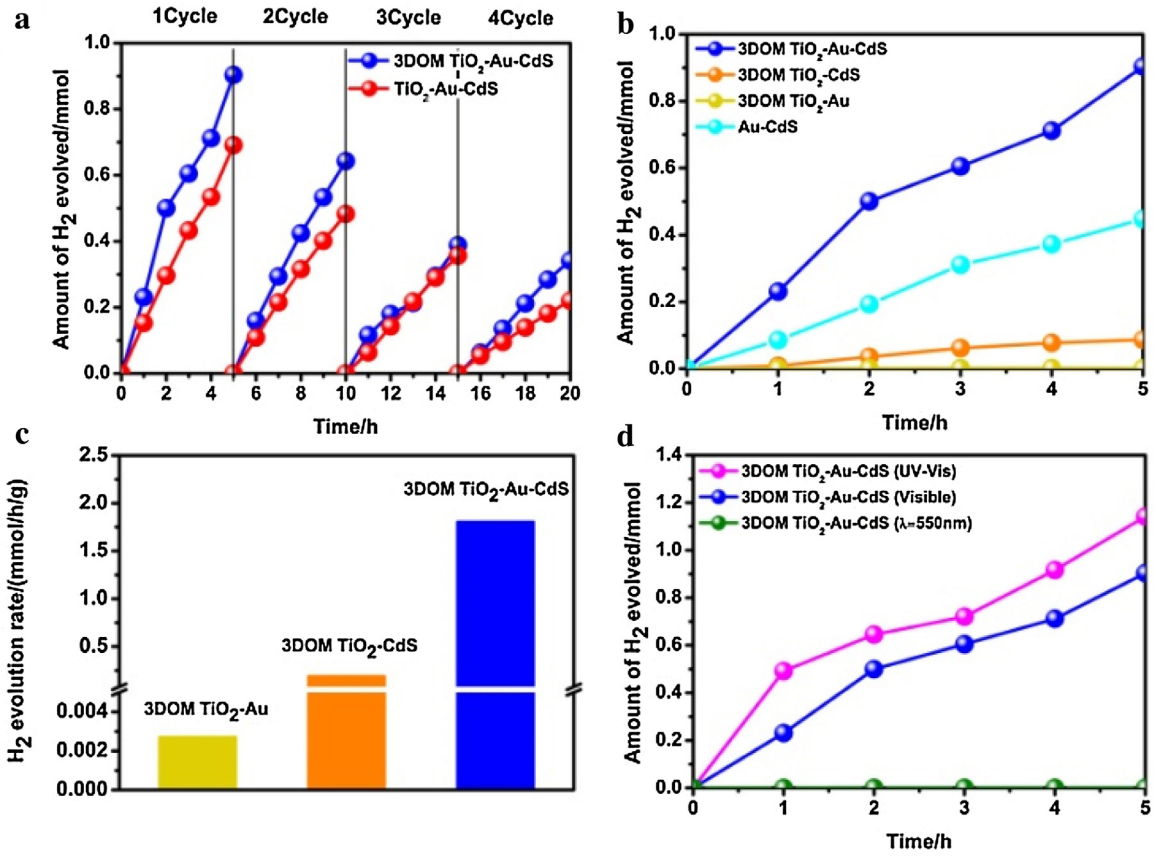

Fig. 8. Photocatalytic hydrogen evolution activities of (a) H_2 evolution of the samples under visible light irradiation for 20 h and every 5 h is a cycle, (b) comparison of H_2 evolution of the samples under visible light irradiation, (c) calculated H_2 evolution rates under visible light irradiation, (d) H_2 evolution of the sample under light irradiation with different wavelength ranges.

(Fig. 7e). The S2p peak at 161.5 eV is corresponding to S^{2-} of CdS nanoparticles (Fig. 7f), which further confirms the obtained samples are composed of TiO_2, Au and CdS. The peak at 168.7 eV is caused by the Na_2SO_3 or Na_2SO_4 [54] which was generated by the oxidation of S^{2-} and sodium is also detected at low resolution (Fig. 7a).

The ternary 3DOM TiO_2-Au-CdS sample was used for light-driven water splitting for H_2 evolution in an aqueous solution containing 0.1 M Na_2S and 0.1 M Na_2SO_3, which act as the sacrificial agents. TiO_2-Au-CdS without 3DOM structure was also prepared for comparison in which TiO_2 was pure anatase phase.

The effect of 3DOM structure on the amount of H_2-generation and stability of the photocatalysts was evaluated through a cycling test of 3DOM TiO_2-Au-CdS and reference TiO_2-Au-CdS sample. As shown in Fig. 8a, the photocatalytic H_2-generation rate of sample 3DOM TiO_2-Au-CdS in the first cycle is 1.81 mmol h^{-1} g^{-1}, much higher than 1.38 mmol h^{-1} g^{-1} produced by TiO_2-Au-CdS without 3DOM structure, indicating a 31% increase in photocatalytic activity by the contribution of 3DOM structure. It is worth noting that the activity of our 3DOM TiO_2-Au-CdS is approximately 13 times higher than the biomass-derived hierarchical porous CdS-Au-TiO_2 (0.14 mmol h^{-1} g^{-1}) synthesized by Zhou et al. [55]. The 3DOM structure does contribute to photocatalytic performance owing to easy mass transfer of the unique porous skeletal structure, which allows the photogenerated holes of CdS to be timely eliminated by S^{2-} and SO_3^{2-} to increase the separation time of electrons and holes. In addition, the ordered porous network can increase the effective optical path length of incident light due to the multiple reflection in this 3DOM structure, thus generating more electron-hole pairs to split water [16,56,57]. The same surface area around 66 m^2/g obtained for 3DOM TiO_2-Au-CdS and TiO_2-Au-CdS samples suggest very clearly that the difference in photocatalytic activity between those two samples is owing to the 3DOM structure. A smooth decrease of H_2-generation rate was observed for both of the samples as the result of the progressive consumption of the sacrificial agents. When the concentration of S^{2-}/SO_3^{2-} becomes very low and is unable to efficiently afford to scavenge the photogenerated holes, S^{2-} in CdS rather than H_2O is oxidized by holes, which is called photocorrosion and the oxidized CdS would lose its photoreactivity.

It is noted that pure anatase TiO_2 is unable to generate H_2 under visible-light irradiation due to the inherent bandgap. AuNPs in the sample 3DOM TiO_2-Au would play a significant role in H_2 generation due to its SPR effect. However, contrary to our expectation, 3DOM TiO_2-Au showed an extremely low H_2 production rate (0.0026 mmol h^{-1} g^{-1} shown in Fig. 8b), revealing that a direct contribution of photocatalytic activity from AuNPs SPR is not noted in our study. This suggests that the presence of both CdS and AuNPs is essential of the photocatalyst in the H_2 generation under visible light irradiation. As a matter of fact, we observed a 68-fold increase of H_2 generation (0.18 mmol h^{-1} g^{-1}) if Au is replaced by CdS in the binary 3DOM TiO_2 photocatalyst. A further 10-fold increased H_2 evolution rate (1.81 mmol h^{-1} g^{-1}) of the ternary photocatalyst 3DOM TiO_2-Au-CdS was observed when AuNPs were introduced to 3DOM TiO_2-CdS (Fig. 8b). The photoreactivity of sample Au-CdS is between 3DOM TiO_2-CdS and 3DOM TiO_2-Au-CdS revealing that TiO_2 skeleton does play a role in the photocatalytic hydrogen evolution under visible light irradiation although TiO_2 can't be excited. The photocatalytic hydrogen evolution activities for the samples based on 3DOM TiO_2 involve light absorption, photogenerated

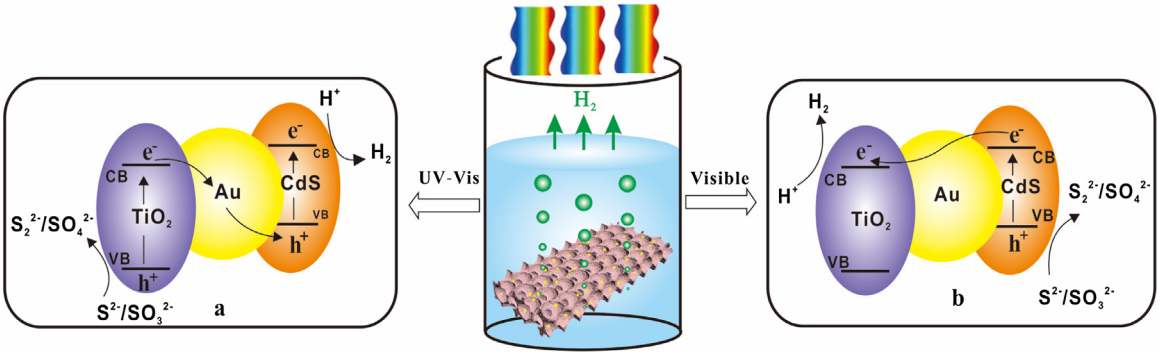

Fig. 9. Illustration of photocatalytic hydrogen evolution over ternary 3DOM TiO_2-Au-CdS under Xenon lamp irradiation. The middle part shows the interaction between light and photocatalyst dispersed in the Na_2S/Na_2SO_3 aqueous solution. The left and right parts illustrate the two different internal electron-transfer processes under ultraviolet-visible light (a) and visible light (b) irradiation respectively.

charge separation and transfer, and reduction reaction on the surface. The enhanced performance of 3DOM TiO_2-Au-CdS compared to 3DOM TiO_2-CdS and Au-CdS could be attributed to the internal electron-transfer process, which is schematically described in Fig. 9.

The photogenerated electrons of CdS under visible light irradiation are transferred from the conduction band of CdS to that of TiO_2 via Au nanoparticles, while holes accumulate at the valence band of CdS (Fig. 9b) to keep the electrons and hole spatially separated. These charge separation processes are very fast [58]. The process of internal electron transfer could be highly accelerated in the presence of AuNPs. H^+ is reduced on the surface of TiO_2 and oxidation reaction occurs on the surface of CdS. The spatially further separation of the electrons and holes in the ternary photocatalyst would result in higher H_2 generation rate than the Au-CdS sample. Besides, AuNPs could act as an electron reservoir due to the lower Fermi levels and photosensitizer due to the SPR effect to reduce H^+ to H_2 on the surface of AuNPs [8]. Compared with 3DOM TiO_2-CdS, there would be more active sites in ternary photocatalyst for reacting with H^+ to produce H_2.

To investigate the effect of incident light, we carried out additional photocatalytic tests controlling the irradiation wavelengths (Fig. 8d). When the sample 3DOM TiO_2-Au-CdS was under ultraviolet-visible light irradiation, there was apparently larger amount of H_2 generation with a rate of 2.28 mmol h^{-1} g^{-1} compared to the case with the visible light irradiation. That is because the internal electron-transfer process is completely different. The relative positions of band structure of TiO_2 and CdS can be generally described as the following: the CB of CdS is more negative than CB of TiO_2, while the VB of TiO_2 is more positive than VB of CdS (as shown in Fig. 9). When this ternary photocatalyst is irradiated under ultraviolet-visible light, CdS supplies the electron-hole pairs and so does TiO_2 (Fig. 9a). The photogenerated electrons of TiO_2 would move to the valence band of CdS through an Au core, and then recombine with holes of the CdS, which departs the electrons and holes spatially, forming the typical electron-transfer pathway of Z-scheme photocatalyst [22,59–63]. The reduction and oxidation reactions would proceed on the CB of CdS and VB of TiO_2 respectively. Compared with the position of electrons excited by visible-light in which only CdS can be excited to generate electrons and holes, the electrons of CdS will be transferred to the CB of TiO_2 via AuNPs due to the relative CB positions of these two components. Herein, the reduction of H^+ to H_2 proceeds on the CB of TiO_2. As the position of the CB of CdS is more negative than that of TiO_2, CdS possesses stronger reducibility and the photogenerated electrons in Z-scheme type photocatalyst accumulating at the conduction band of CdS could enhance photoreduction rate of H^+ to H_2.

The charge separation and photocatalytic performance enhanced by SPR of AuNPs have been reported [21,64,65]. For our ternary photocatalyst 3DOM TiO_2-Au-CdS, we carried out a photocatalytic test while controlling the irradiation wavelength at 550 nm, which excites the SPR of AuNPs, and no enhancement of H_2 evolution was observed (Fig. 8d). This reveals clearly that the SPR of AuNPs could not provide a significant contribution to the photocatalytic activity in our ternary photocatalyst 3DOM TiO_2-Au-CdS. However, AuNPs played a very important role in our ternary photocatalyst. It is well-known that one of crucial factors that hamper the large-scale application of semiconductors in photocatalysis is the high recombination rate of photogenerated carriers. One solution is to form heterojunction structure which is the basic scheme in designing our photocatalyst. Under visible light irradiation, the photoinduced electrons of CdS will be transferred to the conduction band (CB) of TiO_2 due to the relative CB positions of these two components. This process would be highly accelerated in the presence of AuNPs. Therefore, the separation of electrons and holes could be promoted. Besides, as electron reservoir and photosensitizer, the AuNPs could also act as the active sites for reducing H^+ to H_2. The slow photon effect enhancing the light harvesting and the favorable electron migration to the surface of 3DOM TiO_2 structure needs further investigation.

4. Conclusions

A three-component photocatalyst TiO_2-Au-CdS based on 3DOM TiO_2 was successfully fabricated. The 3DOM structure remarkably promotes H_2-generation rate by improving light harvesting and utilizing its easy mass transfer facilitation. The introduction of CdS and AuNPs not only makes up for the ultraviolet light responsive weakness of TiO_2 but also enhances the separation of photogenerated electrons and holes. The dominant role of AuNPs existing between TiO_2 and CdS is acting as electron reservoirs to transfer the photogenerated electrons and produce more active sites for reducing H^+ to H_2. The contribution to H_2-generation of SPR was not observed. 3DOM TiO_2-CdS showed a 68-fold increase of H_2 generation compared to 3DOM TiO_2-Au and a further 13-fold increase for the ternary photocatalyst. The photogenerated electrons of CdS under visible light irradiation move to the conduction band of TiO_2 via AuNPs while under ultraviolet-visible light, the photogenerated electrons of TiO_2 are transferred to the valence band of CdS and recombine with holes. The two internal electron-transfer processes under ultraviolet and visible light both efficiently promote the separation of photogenerated electrons and holes thus promoting H_2 evolution rate of our photocatalyst.

Acknowledgements

This work is realized in the frame of a program for Changjiang Scholars and Innovative Research Team (IRT_15R52) of Chinese

Ministry of Education. B. L. Su acknowledges the Chinese Central Government for an "Expert of the State" position in the Program of the "Thousand Talents". Y. Li acknowledges Hubei Provincial Department of Education for the "Chutian Scholar" program. This work is also financially supported by Hubei Provincial Natural Science Foundation (2014CFB160, 2015CFB516) and Self-determined and Innovative Research Funds of the SKLWUT (2015-ZD-7).

Appendix A. Supplementary data

Supplementary data associated with this article can be found, in the online version, at http://dx.doi.org/10.1016/j.apcatb.2015.11.018.

References

[1] A. Fujishima, K. Honda, Nature 238 (1972) 37–38.
[2] X.B. Chen, S.H. Shen, L.J. Guo, S.S. Mao, Chem. Rev. 110 (2010) 6503–6570.
[3] M.G. Walter, E.L. Warren, J.R. McKone, S.W. Boettcher, Q.X. Mi, E.A. Santori, N.S. Lewis, Chem. Rev. 110 (2010) 6446–6473.
[4] R.M.N. Yerga, M.C.A. Galvan, F. del Valle, J.A.V. de la Mano, J.L.G. Fierro, ChemSusChem 2 (2009) 471–485.
[5] T.L. Thompson, J.T. Yates, Chem. Rev. 106 (2006) 4428–4453.
[6] H. Yoo, C. Bae, Y. Yang, S. Lee, M. Kim, H. Kim, Y. Kim, H. Shin, Nano Lett. 14 (2014) 4413–4417.
[7] J. Wang, D.N. Tafen, J.P. Lewis, Z.L. Hong, A. Manivannan, M.J. Zhi, M. Li, N.Q. Wu, J. Am. Chem. Soc. 131 (2009) 12290–12297.
[8] T. Butburee, Y. Bai, J. Pan, X. Zong, C. Sun, G. Liu, L. Wang, J. Mater. Chem. A 2 (2014) 12776–12784.
[9] J.T. Li, M.W.G. Hoffmann, H. Shen, C. Fabrega, J.D. Prades, T. Andreu, F. Hernandez-Ramirez, S. Mathur, J. Mater. Chem. 22 (2012) 20472–20476.
[10] M. Shen, Z.P. Yan, L. Yang, P.W. Du, J.Y. Zhang, B. Xiang, Chem. Commun. 50 (2014) 15447–15449.
[11] W.J. Liao, J.W. Yang, H. Zhou, M. Murugananthan, Y.R. Zhang, Electrochim. Acta 136 (2014) 310–317.
[12] D.P. Serrano, G. Calleja, P. Pizarro, P. Galvez, Int. J. Hydrogen Energy 39 (2014) 4812–4819.
[13] L. Liu, S. Ouyang, J. Ye, Angew. Chem. Int. Ed. 125 (2013) 6821–6825.
[14] H. Xu, S. Ouyang, L.Q. Liu, P. Reunchan, N. Umezawa, J. Ye, J. Mater. Chem. A 2 (2014) 12642–12661.
[15] Z.Y. Cai, Z.G. Xiong, X.M. Lu, J.H. Teng, J. Mater. Chem. A 2 (2014) 545–553.
[16] J.I.L. Chen, G. von Freymann, S.Y. Choi, V. Kitaev, G.A. Ozin, Adv. Mater. 18 (2006) 1915–1919.
[17] X.F. Cui, Y.J. Wang, G.Y. Jiang, Z. Zhao, C.M. Xu, Y.C. Wei, A.J. Duan, J. Liu, J.S. Gao, RSC Adv. 4 (2014) 15689–15694.
[18] J.I.L. Chen, G.A. Ozin, J. Mater. Chem. 19 (2009) 2675–2678.
[19] G. von Freymann, S. John, V. Kitaev, G.A. Ozin, Adv. Mater. 17 (2005) 1273–1276.
[20] T. Baba, Nat. Photonics 2 (2008) 465–473.
[21] X. Zhang, Y. Liu, S.T. Lee, S.H. Yang, Z.H. Kang, Energ. Environ. Sci. 7 (2014) 1409–1419.
[22] H. Tada, T. Mitsui, T. Kiyonaga, T. Akita, K. Tanaka, Nat. Mater. 5 (2006) 782–786.
[23] J. Fang, L. Xu, Z.Y. Zhang, Y.P. Yuan, S.W. Cao, Z. Wang, L.S. Yin, Y.S. Liao, C. Xue, ACS Appl. Mater. Interfaces 5 (2013) 8088–8092.
[24] L. Ding, H. Zhou, S. Lou, J. Ding, D. Zhang, H.X. Zhu, T.X. Fan, Int. J. Hydrogen Energy 38 (2013) 8244–8253.
[25] H. Zhou, L. Ding, T.X. Fan, J. Ding, D. Zhang, Q.X. Guo, Appl. Catal. B: Environ. 147 (2014) 221–228.
[26] J.T. Li, S.K. Cushing, P. Zheng, T. Senty, F.K. Meng, A.D. Bristow, A. Manivannan, N.Q. Wu, J. Am. Chem. Soc. 136 (2014) 8438–8449.
[27] Y.C. Wei, J.Q. Jiao, Z. Zhao, J. Liu, J.M. Li, G.Y. Jiang, Y.J. Wang, A.J. Duan, Appl. Catal. B: Environ. 179 (2015) 422–432.
[28] M. Sathish, R.P. Viswanath, Catal. Today 129 (2007) 421–427.
[29] F. Sordello, C. Duca, V. Maurino, C. Minero, Chem. Commun. 47 (2011) 6147–6149.
[30] C.W. Cheng, S.K. Karuturi, L.J. Liu, J.P. Liu, H.X. Li, L.T. Su, A.I.Y. Tok, H.J. Fan, Small 8 (2012) 37–42.
[31] M. Srinivasan, T. White, Environ. Sci. Technol. 41 (2007) 4405–4409.
[32] M. Wu, Y. Li, Z. Deng, B.L. Su, ChemSusChem 4 (2011) 1481–1488.
[33] C.T. Dinh, H. Yen, F. Kleitz, T.O. Do, Angew. Chem. Int. Ed. 53 (2014) 6618–6623.
[34] J.I.L. Chen, G. von Freymann, V. Kitaev, G.A. Ozin, J. Am. Chem. Soc. 129 (2007) 1196–1202.
[35] J.S. Jang, H.G. Kim, U.A. Joshi, J.W. Jang, J.S. Lee, Int. J. Hydrogen Energy 33 (2008) 5975–5980.
[36] H. Borchert, E.V. Shevehenko, A. Robert, I. Mekis, A. Kornowski, G. Grubel, H. Weller, Langmuir 21 (2005) 1931–1936.
[37] L.Q. Liu, S.X. Ouyang, J.H. Ye, Angew. Chem. Int. Ed. 52 (2013) 6689–6693.
[38] J. Oh, Y.W. Chang, H.J. Kim, S. Yoo, D.J. Kim, S. Im, Y.J. Park, D. Kim, K.H. Yoo, Nano Lett. 10 (2010) 2755–2760.
[39] A.L. Schmucker, N. Harris, M.J. Banholzer, M.G. Blaber, K.D. Osberg, G.C. Schatz, C.A. Mirkin, ACS Nano 4 (2010) 5453–5463.
[40] S.T. Kochuveedu, D.P. Kim, D.H. Kim, J. Phys. Chem. C 116 (2012) 2500–2506.
[41] J.S. Jang, S.M. Ji, S.W. Bae, H.C. Son, J.S. Lee, J. Photochem. Photobiol. A: Chem. 188 (2007) 112–119.
[42] I. Honma, T. Sano, H. Komiyama, J. Phys. Chem. 97 (1993) 6692–6695.
[43] Y. Ma, X.L. Wang, Y.S. Jia, X.B. Chen, H.X. Han, C. Li, Chem. Rev. 114 (2014) 9987–10043.
[44] W.F. Zhang, M.S. Zhang, Z. Yin, Q. Chen, Appl. Phys. B-Lasers O 70 (2000) 261–265.
[45] J.W. Ng, S.P. Xu, X.W. Zhang, H.Y. Yang, D.D. Sun, Adv. Funct. Mater. 20 (2010) 4287–4294.
[46] Y. Lei, L.D. Zhang, G.W. Meng, G.H. Li, X.Y. Zhang, C.H. Liang, W. Chen, S.X. Wang, Appl. Phys. Lett. 78 (2001) 1125–1127.
[47] H. Nakajima, T. Mori, Q. Shen, T. Toyoda, Chem. Phys. Lett. 409 (2005) 81–84.
[48] B. Liu, L. Wen, X. Zhao, Mater. Chem. Phys. 106 (2007) 350–353.
[49] Y.X. Zhang, G.H. Li, Y.X. Jin, Y. Zhang, J. Zhang, L.D. Zhang, Chem. Phys. Lett. 365 (2002) 300–304.
[50] N.D. Abazovic, M.I. Comor, M.D. Dramicanin, D.J. Jovanovic, S.P. Ahrenkiel, J.M. Nedeljkovic, J. Phys. Chem. B 110 (2006) 25366–25370.
[51] L.Q. Jing, Y.C. Qu, B.Q. Wang, S.D. Li, B.J. Jiang, L.B. Yang, W. Fu, H.G. Fu, J.Z. Sun, Sol. Energy Mater. Sol. Cell 90 (2006) 1773–1787.
[52] S.Q. Liu, N. Zhang, Z.R. Tang, Y.J. Xu, ACS Appl. Mater. Interfaces 4 (2012) 6378–6385.
[53] Y. Yu, H.H. Wu, B.L. Zhu, S.R. Wang, W.P. Huang, S.H. Wu, S.M. Zhang, Catal. Lett. 121 (2008) 165–171.
[54] J.G.A. Terlingen, J. Feijen, A.S. Hoffman, J. Colloid Interface Sci. 155 (1993) 55–65.
[55] H. Zhou, J.Y. Pan, L. Ding, Y.W. Tang, J. Ding, Q.X. Guo, T.X. Fan, D. Zhang, Int. J. Hydrogen Energy 39 (2014) 16293–16301.
[56] H. Xu, X. Chen, S.X. Ouyang, T. Kako, J.H. Ye, J. Phys. Chem. C 116 (2012) 3833–3839.
[57] J.I.L. Chen, E. Loso, N. Ebrahim, G.A. Ozin, J. Am. Chem. Soc. 130 (2008) 5420–5421.
[58] V.M. Daskalaki, M. Antoniadou, G.L. Puma, D.I. Kondarides, P. Lianos, Environ. Sci. Technol. 44 (2010) 7200–7205.
[59] H.J. Yun, H. Lee, N.D. Kim, D.M. Lee, S. Yu, J. Yi, ACS Nano 5 (2011) 4084–4090.
[60] J. Xian, D. Li, J. Chen, X. Li, M. He, Y. Shao, L. Yu, J. Fang, ACS Appl. Mater. Interfaces 6 (2014) 13157–13166.
[61] K. Maeda, ACS Catal. 3 (2013) 1486–1503.
[62] H.M. Zhu, B.F. Yang, J. Xu, Z.P. Fu, M.W. Wen, T. Guo, S.Q. Fu, J. Zuo, S.Y. Zhang, Appl. Catal. B: Environ. 90 (2009) 463–469.
[63] P. Zhou, J.G. Yu, M. Jaroniec, Adv. Mater. 26 (2014) 4920–4935.
[64] S.W. Cao, Z. Yin, J. Barber, F.Y.C. Boey, S.C.J. Loo, C. Xue, ACS Appl. Mater. Interfaces 4 (2012) 418–423.
[65] R.B. Jiang, B.X. Li, C.H. Fang, J.F. Wang, Adv. Mater. 26 (2014) 5274–5309.